Spectrophotometric and Digital Colour Colourimetric (DCC) analysis of Colour-based Indicators

Yusufu, D., & Mills, A. (2018). Spectrophotometric and Digital Colour Colourimetric (DCC) analysis of Colour-based Indicators. *SENSORS AND ACTUATORS B-CHEMICAL*, *273*, 1187 -1194. https://doi.org/10.1016/j.snb.2018.06.131

Published in:
SENSORS AND ACTUATORS B-CHEMICAL

Document Version:
Peer reviewed version

Spectrophotometric and Digital Colour Colourimetric (DCC) analysis of Colour-based Indicators

Dilidaer Yusufu and Andrew Mills*

School of Chemistry and Chemical Engineering, Queens University Belfast, BT9 5AG

e-mail: andrew.mills@qub.ac.uk

Key words: digital photography; spectrophotometry; *RGB*; colour analysis; colour indicators

Abstract

Seven simulated absorption spectra that span the visible spectrum, are used to probe the degree of linear correlation that exists between real absorbance, A_o, at λ_{max}, and three well-established colour-based parameters, based on the standard Red, Green and Blue scale, *sRGB*, namely: (i) apparent absorbance, A(*sRGB*), (ii) apparent fraction of absorbed light, 1-T(*sRGB*), where T is the apparent transmittance and (iii) colour difference, ΔE. In all cases the colour-based parameter, A(*sRGB*), linearly correlates best with A_o. This predicted correlation is tested using three different, actual colour-based indicators, using UV/Vis absorption spectroscopy to monitor the change in actual absorbance of each of the indicators and digital photography to monitor simultaneously the change in the values of *sRGB*, and so A(*sRGB*). The three different indicators used were: a CO_2 indicator, a photocatalytic activity indicator and an oxygen indicator. In all three cases the apparent absorbance parameter, A(*sR*), derived from *sRGB* analysis of the digital images, is proportional to the real absorbance, as measured using UV/Vis spectrophotometry, and able to yield the same key analytical information. The increasing use of *sRGB* analysis of digital photographic images, i.e. digital colour colourimetry, DCC, is discussed briefly.

Introduction

There is a great deal of interest in optical sensors and probes, which are able to respond reversibly, or irreversibly, to specific analytes [1]. In many cases the optical effect is a colour change measured using UV/Vis absorption spectroscopy, where a change in the measured absorbance at a specific wavelength, A_λ, is usually related simply to a change in concentration of the analyte under test. However, even when used in a very basic form, UV/Vis spectroscopy is not an inexpensive technique, nor is it particularly portable, both of which add to the overall cost of analysis when using optical sensors.

Interestingly, there is a recent and growing interest in the use of digital photography, coupled with digital image analysis, to probe colour changing reactions that are so often studied using UV/Vis spectroscopy. For example, Knutson *et al.* have used digital photography to study the kinetics of reaction between crystal violet and hydroxide ions [2]. Wang *et al.* have used a mobile phone's digital camera to probe the colour change associated with a .microchip enzyme-linked immunosorbent assay, ELISA, when exposed to different levels of the ovarian HE4 biomarker in urine [3]. Capitan-Vallvey *et al.* have used colour digital photography for one-shot, multi-ion (potassium, magnesium and hardness) detection [4] and Ozcan *et al.* have used mobile phone microscopy for high resolution pathology imaging [5]. And finally and most recently, photography has been used monitor an epidermal UV colorimetric dosimeter and is now the basis of L'Oreal's 'My Patch' UV dosimeter, which involves monitoring UV dose with a mobile phone digital camera coupled to an App [6]. Interestingly, in several of the different examples cited above the method used to relate the digital photographic data to the analyte concentration was different. The above approach to quantitative analysis *via* digital image analysis, has been termed ‘digital camera colourimetry', which we shall refer to henceforth as DCC, given its clear link with conventional colourimetery and its use of simple (non-spectrophotometric) devices, such as the filter photometer [7, 8].

Colour has been precisely defined internationally and standards have been developed to ensure accurate colour representation [9, 10]. Thus, the International Colour Consortium, ICC, have defined a device-independent, standard Red (*R*), Green (*G*) and Blue (*B*) colour space, *sRGB*, where any colour in that colour space is defined by the values of *R*, *G* and *B*, each of which ranges from zero to 255 (i.e. *8 bit* format), or 0 to 1 (sometimes referred to

as: *fractional* format) [11]. Whatever the format, often these values are referred to as 'intensities' and this terminology will be adopted here, since, as we shall see, they are used in DCC to generate apparent absorbance and transmittance values, i.e. A(*sRGB*) and T(*sRGB*), respectively, *vide infra*. Many image analysis mobile phone Apps (ColorMeter [12], Color Card [13], and Color Mate [14]) and open source digital image processing programs, such as: ImageJ [15], Adobe Photoshop [16] or Image Colour Picker [17], are able to analyse readily any part of a digital image and return the *non-linear sRGB* values associated with the colour.

As note earlier, in many of the examples of DCC cited above the individual methodologies used to relate the *sRGB* colour data to the analyte concentration were different. For example, Knutson *et al.* [2], in their study of the kinetics of reaction between crystal violet and hydroxide ion, showed that the DCC absorbance parameter for the green component, i.e. A(*sG*), was related directly the concentration of the dye, crystal violet, CV, where:

$$A(sG) = \log(sG_o/sG_{CV}) \qquad (1)$$

and sG_o and sG_{CV} are the digital image 'intensity' values for the *sG* component derived from the photograph of the reaction solution in the absence and presence of the CV, respectively; note: sG_o is usually taken to be equal to 255 (or 1). In contrast, in their use of DCC to quantify the level of HE4 in urine, Wang *et al.* [3] showed that the DCC transmittance for the red component of the digital image, i.e. T(s*R*), was related directly the concentration of HE4, *via* the expression:

$$1\text{-}T(sR) = K[HE4] \qquad (2)$$

where, $T(sR) = sR_{HE4}/sR_o$ and sR_o and sR_{HE4} are the intensity values for the *sR* components of the digital image of the ELISA indicator in the absence and presence of the HE4, respectively. The parameter, 1- T(*sR*), will be referred to here as the apparent fraction of light absorbed by the system. Since the standard red component is not absorbed in absence of HE4, once again it is assumed that the value of sR_o = 255 (or 1 if in *fractional* format). Finally, Araki *et al*. [6], in their use of DCC to determine the UV dose received by the indicator, employed the *sRGB* data, derived from photographic images of the indicator, to calculate the values of *L*, *a* and *b*, in the *Lab* colour scale, and then determine the change in colour between a UV exposed and non-exposed indicator, i.e. ΔE, where:

$$\Delta E = [(L_o - L_x)^2 + (a_o - a_x)^2 + (b_o - b_x)^2]^{1/2} \quad (3)$$

Where the subscripts 'o' and x' refer to the values of *L*, *a* and *b* values derived from the images of the non-exposed and UV-exposed indicator, respectively, where the value L_o, a_o and b_o were assumed to be 1, 0 and 0, respectively.

This paper seeks to identify which of the above three digital image-based parameters, i.e. A(*sRGB*), 1-T(*sRGB*) and ΔE, is best at providing a linear correlation with real absorbance values, as measured using UV/Vis spectrophotometry, at a series of wavelengths that span the visible solar spectrum. Once identified, this DCC analysis best method is combined with digital image recording and *sRGB* calculations, using a mobile phone and App, respectively, to probe the responses of three different known optical sensor systems to see if it is able to generate the same analytical information as that gleaned from a UV/Vis spectrophotometric analysis of the same system.

Experimental

Materials

Unless stated otherwise, all chemicals were purchased from Sigma Aldrich and used as received. The Activ™ self-cleaning glass was a gift from Pilkington Glass. All aqueous solutions we made up with double-distilled, deionised water. All gases were purchased from BOC.

The phenol red (PR) CO_2-sensitive plastic polymer film was prepared as described previously [18], using PR instead of 8-hydroxypyrene-1,3,6-trisulfonic acid trisodium salt (HPTS) as the pH-sensitive dye. Thus, 0.2 g of PR were fully dissolved in a mixture of 3.1 ml of 40% tetrabutylammonium hydroxide, TBAH, aqeous solution and 100 ml of ethanol, after which 2 g of hydrophilic silica were added, and the dispersion stirred for 2.5 h. The final purple powdered form of the PR-TBAH-SiO_2 pigment was then obtained *via* spray-drying the dispersion usinga Buchi B-290 spray dryer. The PR-TBAH-SiO_2 pigment was then mixed with low density polyethylene (LDPE), 5 wt%, and extruded out as a 50 μm thick, 10 cm wide, film using a Rondol Microlab 10 mm twin screw extruder (barrel L/D 25/1). The final purple coloured plastic film changed to a yellow colour upon exposure to 100% CO_2, returning to its original purple colour in the absence of CO_2, i.e. the colour-changing process was reversible.

The preparation of the resazurin, Rz, ink used in this work is described elsewhere [19], but briefly, 1.33 mg of Rz and 133 mg of glycerol were added to 1 mL of a 1.5 wt% aqueous solution of hydroxyethyl cellulose (HEC), (MW = 250k). The ink was stirred for at least 5 h, to ensure thorough mixing and dissolution of the dye, before use. The Activ™ self-cleaning glass samples were coated with the Rz ink, by securing the glass sample to an impression bed (i.e. a clipboard) and drawing down a ca. 2.5 cm line of the ink placed 3 mm from the top edge of the glass sample. A wire wound rod (a 'K-bar' No. 3 [20]) was used to create the draw down film, the final dry thickness of which was ca. 2.1 μm. The Rz-coated Activ™ sample was then irradiated with UV light (2 mW cm^{-2} using a 352 nm broad band UVA black light (BL) lamp, 2 x 15W) and the photocatalysed reduction of the Rz monitored periodically both spectrophotometrically and photographically until no further colour change was observed in the Rz ink, or after a period of 12 min, whichever was the shorter period of time.

The preparation of the oxygen sensitive thionin acetate, Th, ink used in this work was otherwise identical to that of a MB ink described elsewhere [21], and which briefly comprised: 20 mg of thionin acetate, 100 mg of P25 titania and 1 g of glycerol dissolved mixed in with 10 cm^3 of a 5 wt.% of hydroxyethyl cellulose (HEC, average Mw: 123k) solution in double distilled deionised water. This ink was sonicated for at least 30 minutes to ensure thorough dissolution of the soluble components and subsequently spin-coated onto a borosilicate cover slip (2.4 mm in diameter and 0.145 mm thick) at a rotation speed of 2000 rpm, to produce a dried Th ink film of thickness ~2.1 μm. The ink film was then 'activated' to its colourless, oxygen sensitive form by exposing it to UVA irradiation (typical irradiance, 2 mW cm^{-2}, using a 352 nm broad band UVA BL lamp, 2 x 15W)) for, typically, 20 s. The oxygen driven recovery of the *leuco*-thionin to the blue coloured thionin was monitored as a function of time, *t*, by UV-vis spectrophotometry and digital photography.

Methods

All UV/Vis spectra were recorded using a Cary 60 UV/Vis spectrophotometer. All digital images were recorded using the digital camera (12-megapixel) on a 7+ iPhone. All digital images were analysed using either the ColorMeter App [12], or the free ImageJ (v 1.51d) software [15], both yielded the same non-linear values, *sR*′, *sG*′ and *sB*′, which were subsequently processed as described in the text.

Simulated absorption spectra and determination of *sRGB* and *Lab* values

A very simple simulation of the UV/Vis absorption spectrum of an absorbing species, D, which has a wavelength of maximum absorption, λ_{max}, can be generated using the following expression:

$$A_\lambda = A_o.\exp[-\{(\lambda - \lambda_{max})/(0.6.FWHM)\}^2] \quad (4)$$

where A_λ and A_o are the absorbances due to D at λ and λ_{max}, respectively, and FWHM is full width at half maximum of the absorption band, set at 50 nm. Note that according to Beer's law, A_o is proportional to the concentration of D, [D], and can be varied as required. Thus, figure 1 illustrates the simulated absorption spectra for a series of simulated dyes, D, with λ_{max} values set at those associated with the rainbow colours of the solar spectrum, i.e. red, orange, yellow, green, cyan, blue violet, with, in all cases, A_o set at 1.

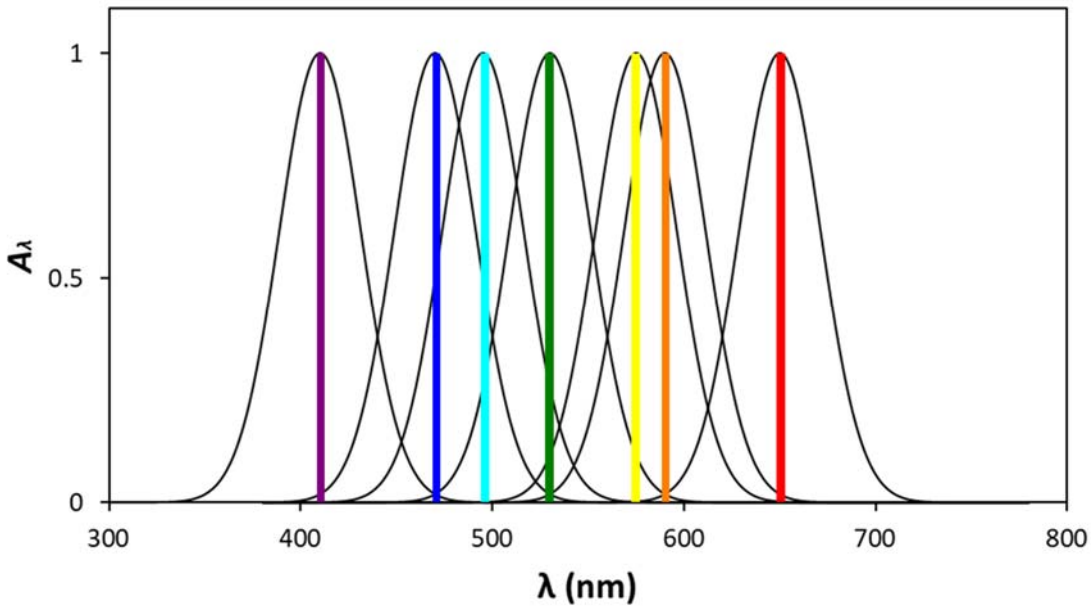

Figure 1: Absorption spectra of seven simulated dyes each absorbing at their λ_{max} values the primary rainbow colours, red, orange, yellow, green, cyan, blue and indigo. Each spectrum was calculated using eqn(4) with A_o = 1.

Knowledge of the absorption spectrum of any light-absorbing species allows its linear *sRGB* values to be calculated and its coloured defined, *via* the three tristimulus values, *X*, *Y* and *Z*, which can be calculated using the following formulae [10]:

$$X = \frac{\sum_\lambda T(\lambda)S(\lambda)x(\lambda)}{\sum_\lambda S(\lambda)y(\lambda)} \quad (5)$$

$$Y = \frac{\sum_\lambda T(\lambda)S(\lambda)y(\lambda)}{\sum_\lambda S(\lambda)y(\lambda)} \quad (6)$$

$$Z = \frac{\sum_\lambda T(\lambda)S(\lambda)z(\lambda)}{\sum_\lambda S(\lambda)y(\lambda)} \quad (7)$$

where $T(\lambda)$ is the transmittance (i.e. $10^{-A\lambda}$) of the simulated dye, $S(\lambda)$ is the spectral power of a standard illuminant (here assumed to be daylight andusually referred to as D_{65}), and $x(\lambda)$, $y(\lambda)$ and $z(\lambda)$ are the two degree standard colour matching functions (CMFs), which are a consequence of the three different cone responses of the eye. Tables of $S(\lambda)$ for D_{65} and $x(\lambda)$, $y(\lambda)$ and $z(\lambda)$ are readily available from the literature [22] and a typical set used here are illustrated in figure 2, and also contained in the 'S1.xls' spread sheet in the supplementary information.

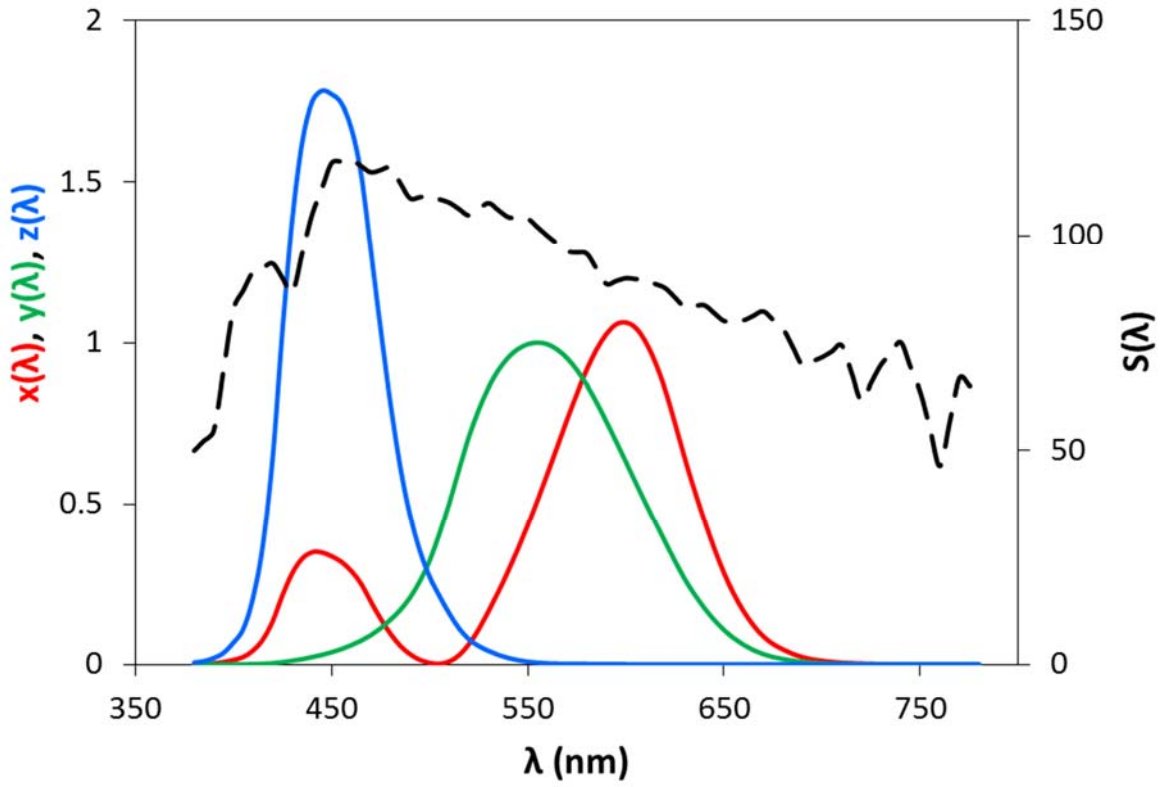

Figure 2: Plots of the known colour matching functions, i.e. $x(\lambda)$, $y(\lambda)$ and $z(\lambda)$ for a 2° standard observer and the $S(\lambda)$ relative spectral power of a standard (D_{65}, i.e. daylight) illuminant as a function of wavelength, λ [20].

Since the value of A_λ at any wavelength, λ, for any of the simulated dyes illustrated in figure 1, can be calculated using eqn (4), given a knowledge of λ_{max}, it follows that each simulated dye absorption spectrum depicted in figure 1, can be defined by a set of tristimulus values, *X*, *Y* and *Z*. These, in turn, can be converted to *sR*, *sG* and *sB* values using the following matrix transformation equation [10]:

$$\begin{bmatrix} sR \\ sG \\ sB \end{bmatrix} = \begin{bmatrix} 3.2410 & -1.5374 & -0.4986 \\ -0.9692 & 1.8760 & 0.0416 \\ 0.0556 & -0.2040 & 1.0570 \end{bmatrix} \begin{bmatrix} X \\ Y \\ Z \end{bmatrix} \quad (8)$$

The above process generates linear *sR*, *sG* and *sB fractional* values in the range 0-1, however, it more usual to convert them to the 24 bit *sRGB* code, [*sR sG sB],* where [0 0 0] is black and [255 255 255] is white. Usually this means multiplying each fractional value by 255 and rounding to nearest whole number, with the caveat that if any fractional value is < 0, then a value of zero is returned and if any is > 1, a value of 255 is returned [10].

Alternatively, the tristimulus values, *X*, *Y* and *Z,* can be converted to *Lab* values using the following equations [6]:

$$L^* = 116f(Y/Y_n) - 16 \tag{9}$$

$$a^* = 500[f(X/X_n) - f(Y/Y_n)] \tag{10}$$

$$b^* = 200[f(Y/Y_n) - f(Z/Z_n)] \tag{11}$$

Where

$$f(t) = \begin{cases} t^{1/3} & \text{if } t > (\frac{6}{29})^3 \\ \frac{1}{3}(\frac{29}{6})^2\, t + \frac{4}{29} & \text{otherwise} \end{cases} \tag{12}$$

Where, for any simulated dye, X_n, Y_n and Z_n are the values of *X*, *Y* and *Z,* calculated using eqns (5-7), respectively, but with $T(\lambda)$ set **always** to be 1. Thus, in this work, it is found that: X_n = 95.047, Y_n = 100.000, Z_n = 108.883 using the D_{65} Illuminant.

Table 1 lists the: (i) *X*, *Y* and *Z,* (ii) *sR*, *sG* and *sB* and (iii) *Lab* and ΔE values calculated for each of the absorption spectra illustrated in figure 1, using equations (5 – 7), (8) and (9) and (3), respectively. In table 1, the colour border used round this data, i.e. (i) – (iii) is how each simulated dye with a maximum absorbance, A_o, = 1 would appear, i.e. as the complimentary colour to that which it is absorbing.

An example spreadsheet, highlighting the calculations involved in the determination of the (i) – (iii) values reported in Table 1 for the yellow-absorbing, i.e. λ_{max} = 575 nm, simulated dye is given in the 'S2.xls' spreadsheet in the supplementary information. Note: in all ΔE value calculations, all colour changes are with reference to white light, for which the values of: L_o, a_o and b_o are: 100, 0 and 0, respectively.

Table 1: Spectral and calculated s(*RGB*), *Lab* and ΔE characteristics of seven simulated dyes spanning the solar spectrum

Colour	Violet	Blue	Cyan	Green	Yellow	Orange	Red
λ_{max} (nm)	410	470	495	530	575	590	650
[X,Y,Z]	[0.88,0.99,0.74]	[0.83,0.90,0.37]	[0.87,0.77,0.69]	[0.80,0.54,1]	[0.53,0.52,1.1]	[0.49,0.60,1.1]	[0.76,0.92,1.1]
sRGB	[244,255,160]	[255,229,65]	[255,158,159]	[255,71,255]	[94,130,255]	[31,177,255]	[128,255,255]
Lab	[97,-12,24]	[95,-5,54]	[97,29,12]	[93,65,-33]	[79,9,-39]	[77,-21,-31]	[92,-22,-6]
*ΔE**	27	54	31	73	45	44	24
PCC**	blue	blue	green	green	red	red	red

*: Reference white point is RGB (255, 255, 255) or Lab (100, 0, 0), where ΔE = 0.
**: Primary colour component.

Correlation studies

The previous section outlines how it is possible to use the associated UV/Vis absorption spectrum to calculate the *sR*, *sG* and *sB* and *Lab* and ΔE values for any of the simulated dyes solutions illustrated in figure 1. Now, for all the simulated dyes illustrated in figure 1, the maximum absorption at λ_{max}, i.e. A_o, was set at 1. However, the same process can also be used to calculate the *sR*, *sG* and *sB* and *Lab* and ΔE values for any of the simulated dyes for any value of A_o, i.e. at any dye concentration. Thus, in this work A_o was varied from 0-1, in steps of 0.05, for each of the simulated dyes to simulate a range of different dye concentrations, and in each case values for *sR*, *sG* and *sB* and *Lab* and ΔE, were calculated using the same procedure as described in the previous section. Spectra for the simulated dyes for which $A_o > 1$ were not studied for, as we shall see, this is too high for DCC to produce any likely correlation with any measured UV/Vis absorbance. In the case of the *sR*, *sG* and *sB* data generated for each simulated dye, usually one of the colours, i.e. *R*, *G* or *B*, varies to a greater extent compared to the other two over the A_o range 0-1. For example, for the yellow-absorbing dye illustrated in figure 1, with λ_{max} = 575 nm, a brief inspection of the variation of the calculated values of *sR*, *sG* and *sB* as a function of A_o, illustrated in figure 3, reveals that the **red** component is most affected by the change of A_o from 0-1. In all this work, for any light absorbing system we shall refer to this component, i.e. the colour component which changes most markedly with change in A_o as the 'primary colour component' or 'PCC' for short. Note: as a rough guide, the PCC is the complementary colour to that of the analytical system under test. Thus, the PCC is red, green or blue for a coloured system that appears approximately cyan, magenta or yellow, respectively [23].

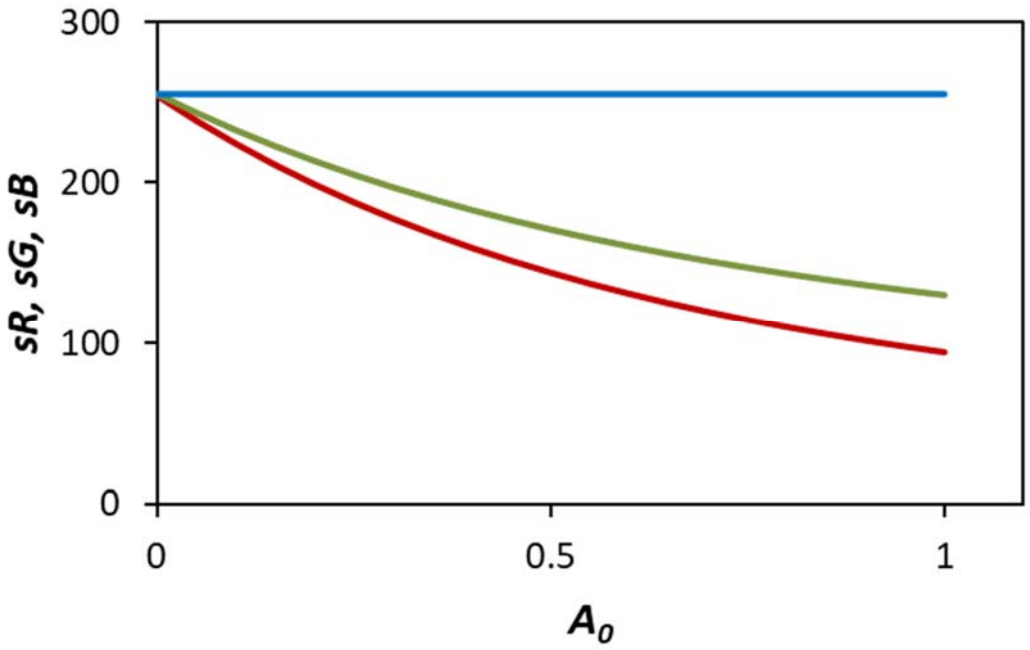

Figure 3: Plots of *sR* (red line), *sG* (green line), and *sB* (blue line), values determined for the yellow-absorbing simulated dye as a function of absorbance at λ_{max}, i.e. A_o, from which it is clear that the red component varies most significantly as the value of A_o is increased from 0 to 1, in steps of 0.05, whilst, in contrast, the blue component remains unchanged at all values of A_o.

As a consequence, since red is the PCC for the yellow absorbing dye (see figure 3), only the red component data were used to calculate values for A(*sR*) and 1-T(*sR*) for the yellow-absorbing simulated dye, using the appropriate versions of equations (1) and (2), respectively, as a function of A_o. In addition, the *sR*, *sG* and *sB* data in figure 3, for the yellow-absorbing simulated dye, was used to calculate values for *Lab,* and so ΔE, also as a function of A_o which was varied over the range 0-1. Plots of these three different data sets, i.e. A(*sR*), 1-T(*sR*)and ΔE vs A_o, for the yellow simulated dye are illustrated in figure 4 from which it appears that the absorbance-like parameter based on the *sR* values, i.e. A(*sR*), provides the best linear correlation, of the three plots, with A_o, and this observation is supported by the near unity value for the square of the correlation coefficient for the line of best fit (i.e. $r^2 = 0.9941$). It is also clear that all three parameters show increasing deviation from linearity as the value of is A_o increased and that even A(*sR*) shows clear signs of deviating significantly at A_o values > 1. This was found to be true for all the simulated dyes tested and so the correlation study was limited to a variation of A_o from 0 to 1, as noted earlier.

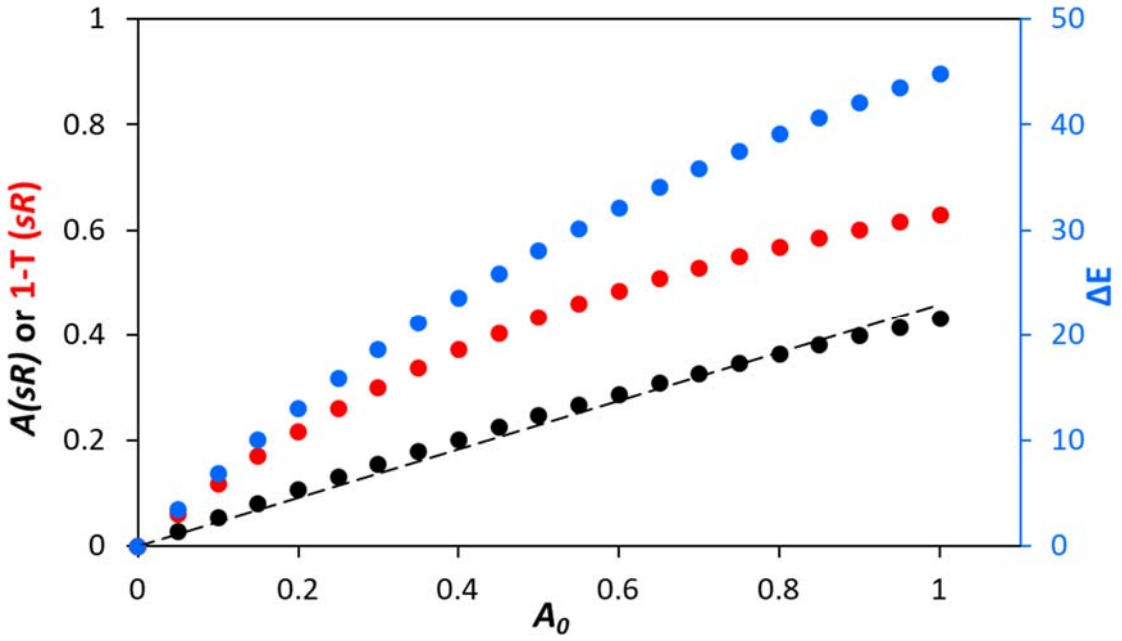

Figure 4: Plots of A(*sR*) (black dots), 1-T(*sR*) (red dots) and ΔE (blue dots) as a function of A_o for the yellow-absorbing simulated dye (see figure 1) calculated using the *sR, sG* and *sB* values illustrated in figure 3. The line of best fit (broken line) for the plot of A(*sR*) vs. A_o yields a correlation coefficient , r^2, 0.9941.

The same procedure was applied to **all** the simulated dyes illustrated in figure 1 and in each case the PCC was identified (see Table 1) and the data associated with the PCC used to generate plots of: A(*sR*), 1-T(*sR*) and ΔE as a function of A_o over the A_o range of 0-1. The square of the correlation coefficient was determined for each of these correlation plots and the results of this work are plotted as a function of λ_{max} in figure 5 for the different simulated dyes. A brief inspection of this plot of correlation coefficient data reveals that, as for the yellow-absorbing dye in figure 4, the absorbance-like parameter, A(*sR, sG* or *sB*), correlates linearly much more closely with A_o, than the other two functions, 1-T(*sR, sG* or *sB*) and ΔE.

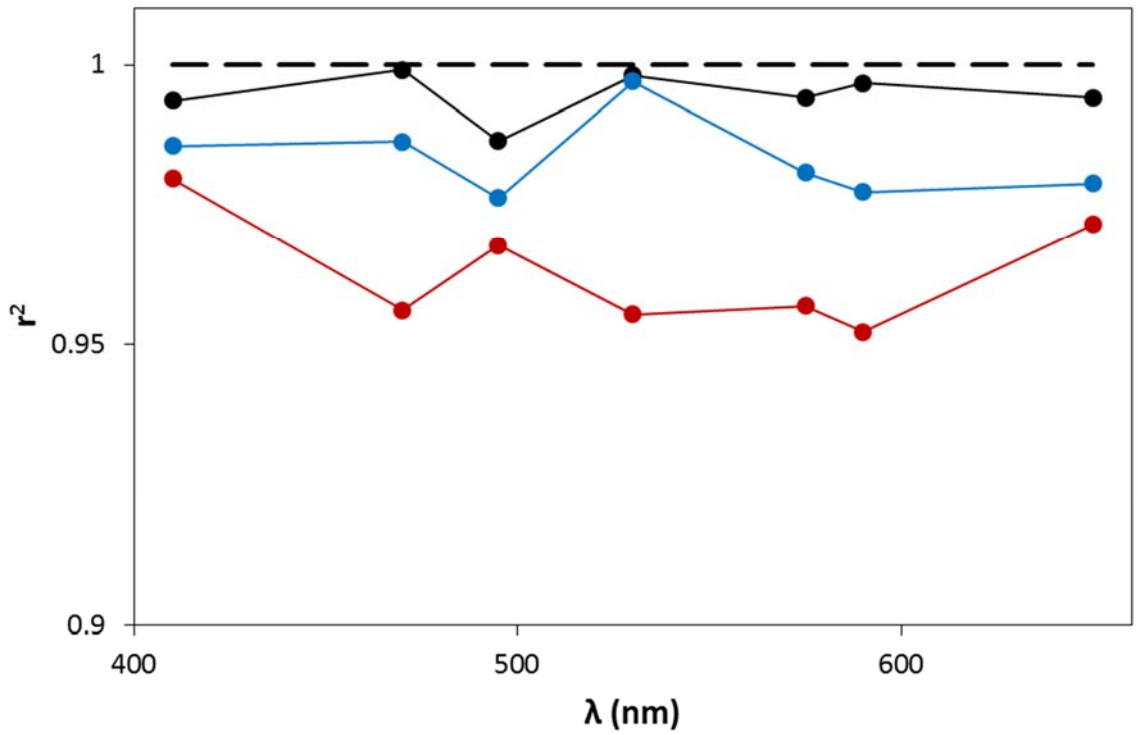

Figure 5: Plots of squares of correlation coefficients, r^2 as a function of λ_{max} for the seven simulated dyes listed in table 1. The individual r^2 values themselves were derived from plots of the *sRGB* PCC data for each of the seven dyes in the form of: A(*sR, sG* or *sB*) (black line), 1-T(*sR, sG* or *sB*) (red line) or ΔE (blue line) vs. A_o.

These results imply that values for the absorbance-like parameter, i.e. A(*sR, G* or *B*), determined from digital photographic data, i.e. *sR*, *sG* or *sB* values, can be used, instead of absorbance values determined using UV/Vis spectrophotometry, as a measure of concentration of the light absorbing species. This is a useful observation given that the cost of DCC is low and the technique very portable, unlike UV/Vis spectroscopy and, also – once in place - the process is simple to effect. In order to test the above hypothesis, derived from studies of simulated dyes, three, well-established colour-based sensors were studied using both the conventional, and costly, UV/Vis spectrophotometric technique and the very inexpensive, increasingly popular, simple method of DCC, using a digital mobile phone camera and a RGB measuring App.

Application of DCC to established optical sensor systems

(1) CO_2-sensitive indicators

A large number of CO_2-sensitive, colour-based indicators have been developed and commercialised for various applications, including correct tracheal intubation [24] and environmental monitoring in air and water [25-28]. In most cases the colour changing process is due to the following equilibrium reaction:

$$D^- + H_2O + CO_2 \rightleftharpoons DH + HCO_3^- \quad (13)$$

where D^- and DH are the deprotonated and protonated forms, respectively, of a pH sensitive dye, such as phenol red, PR. It follows that in the presence of an excess of bicarbonate, the concentrations of D^- and DH are related to the ambient level of CO_2, i.e. *via* an expression of the form:

$$[DH]/[D^-] = K.\%CO_2 \quad (14)$$

Where, [DH] and $[D^-]$ are the concentrations of the protonated and deprotonated forms of the pH dye, respectively, and *K* is the proportionality constant which provides a measure of the sensitivity of the sensor towards CO_2. If, as is usually the case, the absorbance of the indicator is measure at a wavelength where only D^- absorbs, which is usually λ_{max} for D^-, i.e. $A(D^-)$, then, according to eqn (14) and Beer's law, $A(D^-)$ will decrease as $\%CO_2$ is increased. It also follows that a plot of $1/A(D^-)$ vs $\%CO_2$ will yield a straight line with a gradient, *K* [29, 30]. However, a much simpler, although more approximate method for assessing the value of *K* is to measure the $\%CO_2$ necessary to create equal concentration of [DH] and $[D^-]$, i.e. $\%CO_2(S = ½)$, since it is equal to the reciprocal of *K*. Note: at $\%CO_2(S = ½)$, $A(D^-) = A(D^-)_o/2$, where $A(D^-)_o$ is the initial absorbance of the indicator [31].

In this work the optical responses of a typical PR-based CO_2-sensitive plastic film sensor, towards different levels of CO_2, were measured using both a UV/Vis spectrophotometer and a mobile phone digital camera and the results of this work are illustrated in figure 6 [32].

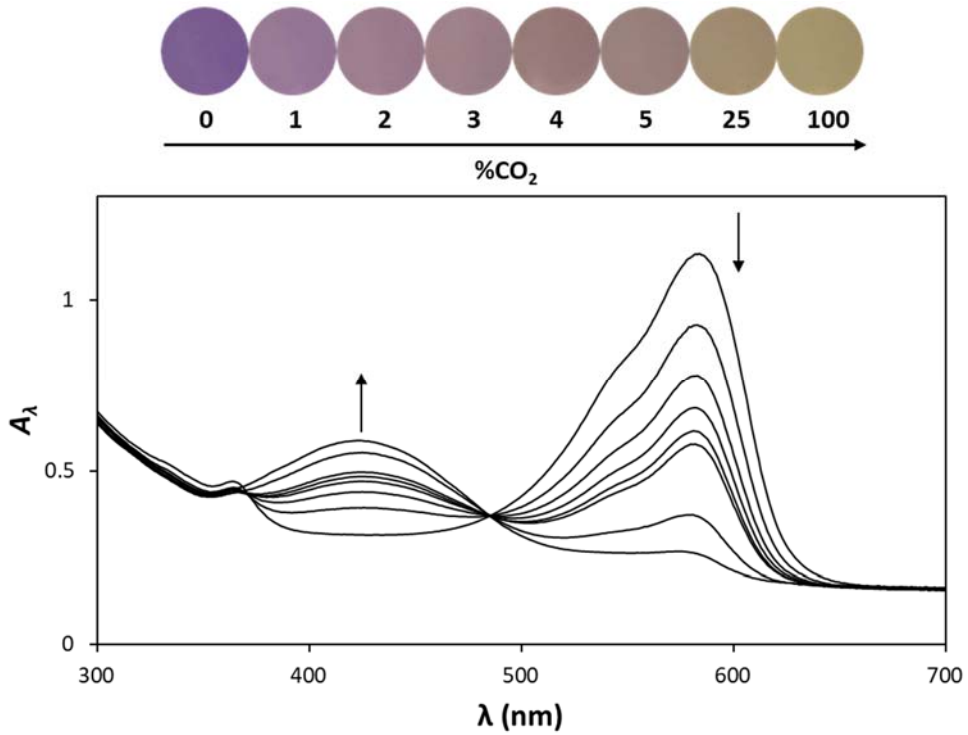

Figure 6: UV/Vis absorption spectra and digital photographic images recorded for a PR-based CO_2 sensitive plastic film as a function of increasing levels of $\%CO_2$ in the gas phase.

The UV/Vis absorbance data in figure 6 is for the PR film at the λ_{max} for its deprotonated form (582 nm) was then plotted as a function of $\%CO_2$ as illustrated in figure 7, from which a value for $\%CO_2$(S = ½), and so *K,* were gleaned for the PR CO_2 indicator film. Similarly, the ColorMeter App on the mobile phone was used to analyse each of the digital photographs taken of the film as a function of $\%CO_2$ and illustrated in figure 6. The *sRGB* values extracted using the App are gamma corrected, *non-linear* parameters, i.e. *sR', sG'* and *sB'* values. In this, and all the other indicators described in this section, the PCC was red and the conversion from the App measured *sR' non-linear* values associated with the digital photographs illustrated in figure 6, to their *linear, sR,* counterparts used the following function:

$$\text{If } sR' \leq 0.0405, \text{ then } sR = 12.92.\ R', \text{ otherwise } sR = \{(sR' + 0.055)/1.055\}^{2.4} \qquad (15)$$

where *sR'* and *sR* are in their fractional (i.e. 0-1) forms, rather than their more usual 8 bit (0-255) forms. Once *sR'* and *sR* were converted to their *linear* values, using eqn (15), then the value of A(*sR*) associated with each of the indicator photographs illustrated in figure 6 was determined and a plot constructed of A(*sR*) vs $\%CO_2$, which is illustrated in figure 7. As an

example, s*RGB* analysis (using the App) of the image of the CO_2 indicator at 2% CO_2 reveals a value of *sR'* of 0.59 (or 150 in 8 bit form), which translates to a value of 0.30 (or 77 in 8 bit form) for *sR*, calculated using eqn (15), and a value of 0.52 for A(*sR*), based on eqn (1), assuming sR_o = 255.

A quick comparison of the two plots in *figure 7,* namely absorbance, A_{582}, (at λ_{max} PR; i.e. 582 nm, measured spectrophotometrically and taken from the spectral changes in figure 6) vs %CO_2 and A(*sR*) (calculated as in eqn (1) using *sR* values derived from the digital images in figure 6) vs %CO_2 reveals that they are near identical in shape, implying –as predicted in the first section – that in practice spectrophotometric absorbance, A_{582}, and the apparent absorbance parameter, A(*sR*), based on digital image analysis, are linearly correlated in this system. As you would expect, given the linear correlation between A_{582}, and the DCC parameter, A(*sR*), both plots of A_{582} and A(*sR*) vs %CO_2 yielded the same value of 2.7 % for %CO_2(S = ½), as illustrated in figure 6. Thus, the solid line in figure 7 is based on eqn (14), assuming a value of *K* = 0.37 $\%^{-1}$, which predicts the value of %CO_2(S = ½) = 2.7%.

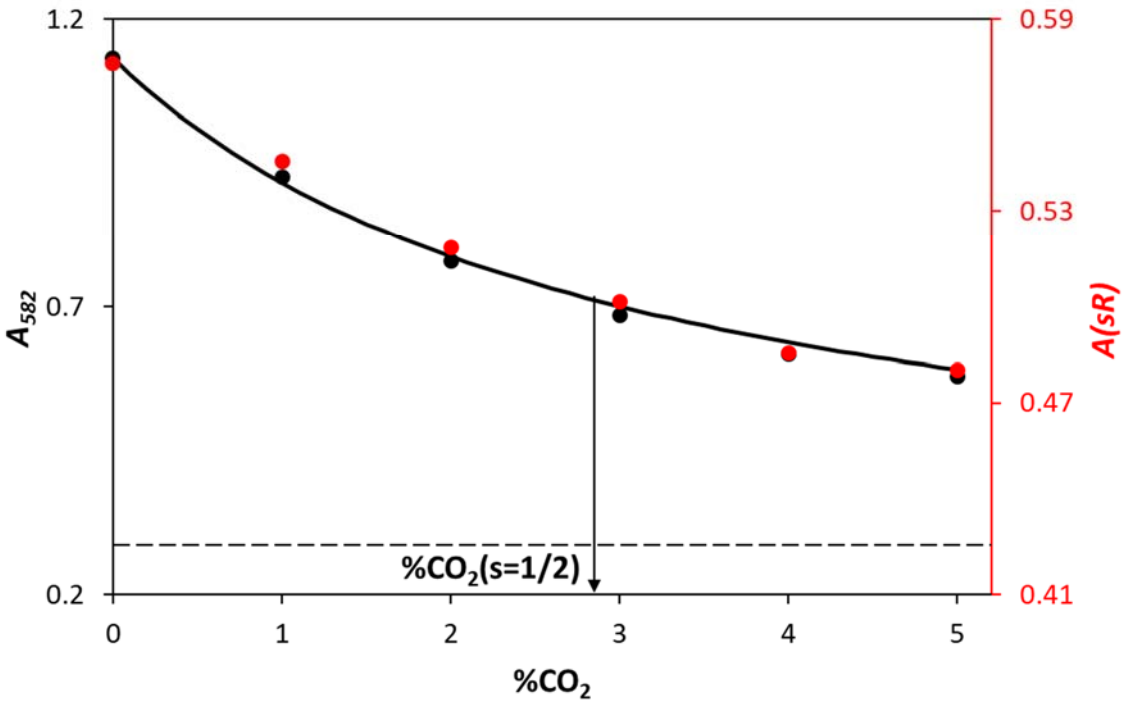

Figure 7: Plots of: (i) absorbance (at λ_{max} PR; measured spectrophotometrically and taken from the spectral changes in figure 6) vs %CO_2 (black data points) and A(*sR*) (calculated as in eqn (1) using *sR* values derived from the digital images in figure 6) vs %CO_2 (red data points). The broken line identifies the values of A_{592} and A(*sR*), when the indicator is exposed to 100% CO_2, so that all the PR is in its protonated form. The solid line was generated using eqn (14), with *K* = 0.37 $\%^{-1}$, which yields a value of %CO_2(S = ½) of 2.7%,

(*2) Photocatalyst activity sensitive indicators*

In recent years a number of new, so called 'self-cleaning' architectural materials have been developed in the form of glass (e.g. Activ® from Pilkington Glass) [33], paint (e.g. Climisan® from STO) [34], concrete (e.g. TX Active® from Italcementi) [35] and tiles (e.g. Hydrotect® from TOTO) [36]. In all cases the active ingredient is photoactive TiO_2, which absorbs UV light and is able to effect the complete mineralisation of most organic contaminants which have deposited onto its surface, i.e.

$$\text{Pollutant} + O_2 \xrightarrow[\text{UV}]{TIO_2} \text{minerals (such as: } H_2O, CO_2 \text{ and acids)} \qquad (16)$$

The above process is an example of semiconductor photocatalysis [37]. There are a growing number of commercial and research photocatalytic materials and so there is a real need for methods to assess the photocatalytic activity. As a consequence a number of international standard testing methods have been developed for this purpose, however most are slow (usually take hours) and are laboratory based, and so not conducive to testing samples *in situ* [38]. Recently a new colourimetric method of assessing photocatalytic activity has been reported [39, 40] based the photocatalysed reduction of a blue dye, resazurin, Rz, to a pink coloured product, resorufin, Rf, *via* the following photocatalytic reaction:

$$\text{glycerol} + \text{Rz} \xrightarrow[\text{UV}]{TiO_2} \text{glyceraldehyde} + \text{Rf} \qquad (17)$$

The rate of photo-induced change in colour of the Rz ink film is proportional to the activity of the underlying photocatalytic material under test. The test is easy to use, fast, i.e. usually < 10 min, and can be used in the *in situ* assessment of photocatalytic materials [41, 42]. In addition, it is now the basis of a recent ISO (DIS 21066) [43], in which the time taken for the

Rz to lose 90% of its colour, *ttb(90)*, is measured, and taken as an inversely proportional measure of the activity of the photocatalyst.

Here the Rz ink was used to probe the activity of a piece of Activ® self-cleaning glass using both a UV/Vis spectrophotometer and a mobile phone digital camera to monitor the change in colour of the Rz ink film (blue to pink) as a function of UV irradiation time and the results of this work are illustrated in figure 8.

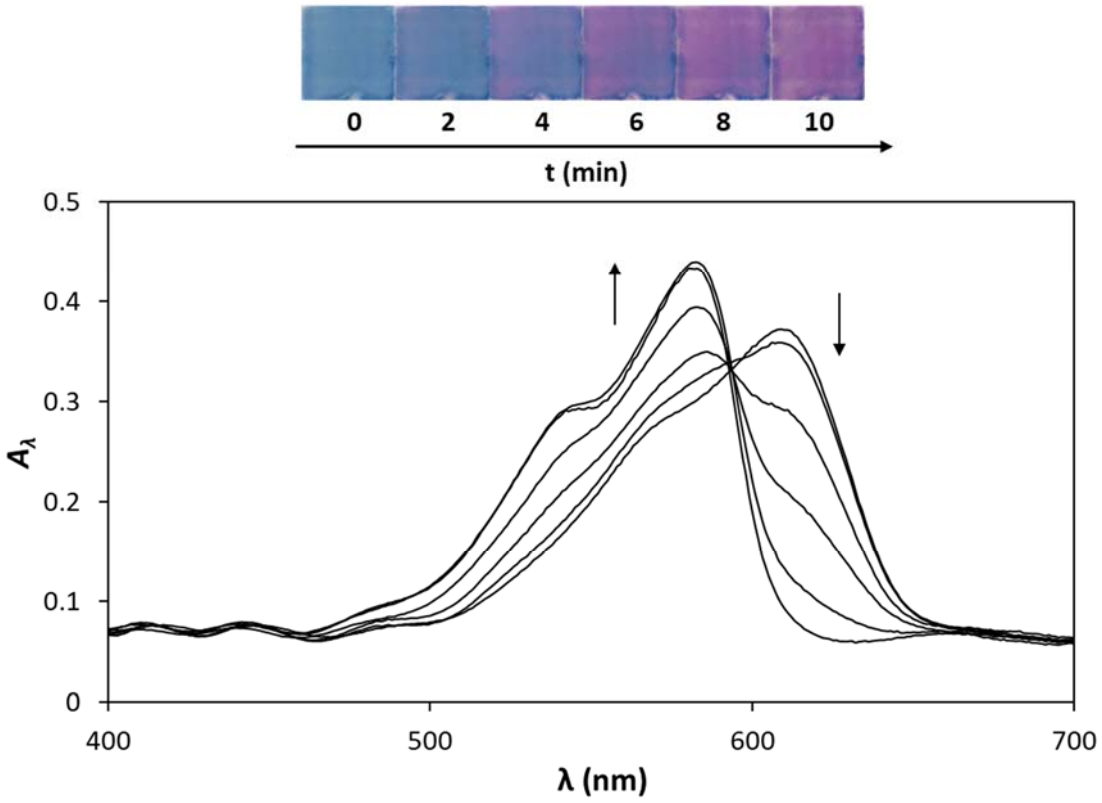

Figure 8: UV/Vis absorption spectra and digital photographic images recorded for a Rz ink on a piece of Activ® glass as a function of UV irradiation time.

The parameter *ttb(90)* can be determined for the Activ® glass by plotting the change in absorbance due to the Rz at its λ_{max} = 609 nm, i.e. A_{609}, as a function of irradiation time, as illustrated in figure 9, where $\Delta A_{t=0}$ is the overall change in A_{609} as the indicator turns from blue to pink due to reaction (17), and *ttb(90)* is the UV irradiation time taken for ΔA = 0.9. $\Delta A_{t=0}$. Using the same data manipulation process as described in the previous section, the photographic images in figure 8 of the Rz ink film were used to generated the plot of A(*sR*) vs UV irradiation time, also illustrated in Figure 9. As before, a quick comparison of the two

plots in figure 9, namely absorbance, A_{609} (at λ_{max} Rz, i.e. 609 nm; measured spectrophotometrically and taken from the spectral changes in figure 8) and *A*(*sR*) (calculated as in eqn (1) using *sR* values derived from the digital images in figure 8) vs UV irradiation time reveals that the spectrophotometric absorbance and *A*(*sR*) data are linearly correlated, as the data points lie on a common line. As a consequence the two data sets generate the same value for *ttb(90)*, namely, ca. 8.6 min.

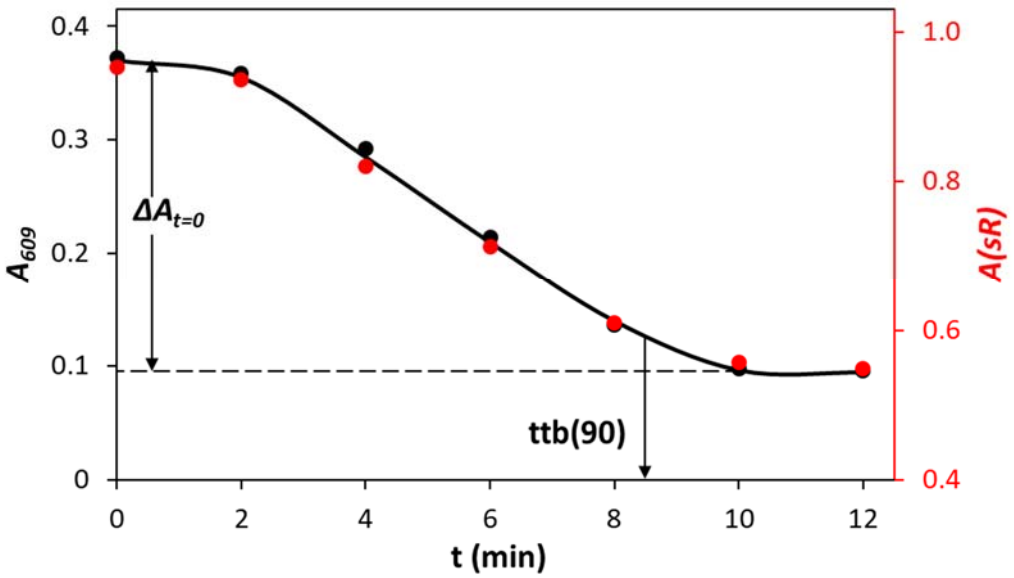

Figure 9: Plots of: (i) absorbance (at λ_{max} Rz; measured spectrophotometrically and taken from the spectral changes in figure 8) vs $\%CO_2$ (black data points) and A(*sR*) (calculated as in eqn (1) using *sR* values derived from the digital images in figure 8) vs UV irradiation time (red data points). Both data sets identify the same value for *ttb(90),* namely 8.6 min.

(3) UV-activated, O_2-sensitive indicators

Probably the most commonly analysed chemical species is O_2, which is not surprising given its key role in many biochemical and chemical processes. In terms of indicators the detection of oxygen is dominated both commercially and in the academic literature by luminescence quenching [44]. Examples of commercial O_2 indicators based on this technology include: Oxydot® from oxysese [45], Spot SP® series from PreSense [46], OpTech® O_2 from Mocon [47], RedEye® oxygen sensor patches from OceanOptics [48]. In contrast, there are few colour-based O_2 indicators [49], although this group has recently developed a UV-activated colour-based oxygen indicator that utilises an ink containing a semiconductor photocatalyst (usually TiO_2), a highly coloured redox dye, usually a thiazine

dye such as methylene blue, MB or thionine, Th, and a sacrificial electron donor, usually glycerol. Upon an initial illumination with UV the ink is 'activated' – i.e. rendered O_2-sensitive, *via* the following photocatalytic process:

$$\text{glycerol} + \text{MB} \xrightarrow[\text{UV}]{\text{TiO}_2} \text{glyceraldehyde} + \text{LMB} \qquad (18)$$

since the reduced form of MB, i.e. *leuco*-methylene blue, LMB, reacts readily with O_2, via:

$$\text{LMB} + \text{O}_2 \longrightarrow \text{MB} + \text{H}_2\text{O} \qquad (19)$$

Thus, upon exposure to a short, intense burst of UV illumination the initially blue coloured ink is bleached to LMB and stays bleached until and unless O_2 is present, whereupon it regains its original blue colour at a rate, or half-life, *t(50)*, that depends upon the ambient level of O_2 [50]. This indicator technology has been used commercially to identify O_2 ingress in packaged food [51].

In this study, a typical TiO_2/thionine/glycerol ink was used to coat a glass cover slip and, after exposure to a burst of UV light (2 mW cm^{-2} for 20 s from 2x15 W 352 nm BL lamps) the recovery of its original colour in air (21% O_2) was monitored both spectrophotometrically and photographically as a function of 'dark' time (i.e. time after the initial exposure to UV radiation) and the results of this work are illustrated in figure 10.

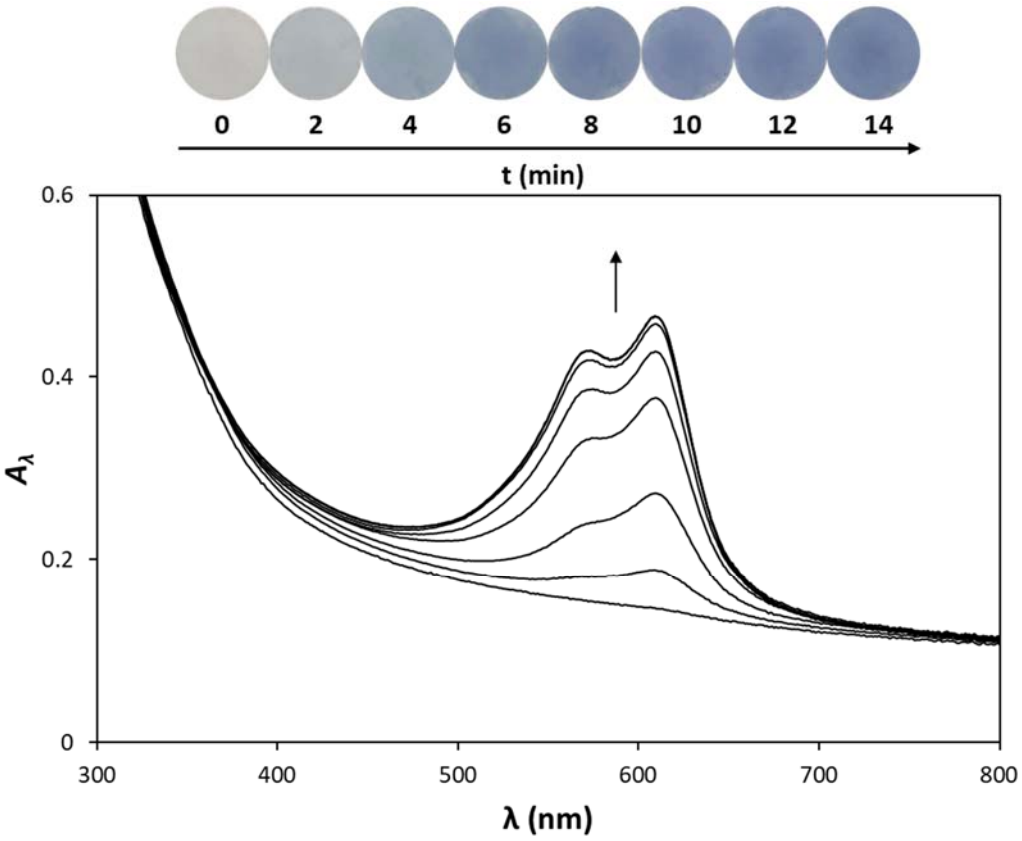

Figure 10: Recovery in air of a photocatalytically-reduced TiO_2/thionine/glycerol ink film monitored both spectrophotometrically and using a digital mobile phone camera. The change in absorbance spectrum of the ink film recorded every 2 mins is illustrated here.

The parameter *t(50)* in air can be determined for the UV-activated TiO_2/thionine/glycerol ink film by plotting the change in absorbance due to the Th in the ink at its λ_{max} = 609 nm, i.e. A_{609}, as a function of 'dark' time, as illustrated in figure 11, where $\Delta A_{t=0}$ is the overall change in A_{609} as the indicator turns from colourless to blue due to reaction (19), and *t(50)* is the time taken for $\Delta A = 0.5 \times \Delta A_{t=0}$. Using the same data manipulation process as described in the previous section, the photographic images in figure 10 of the TiO_2/thionine/glycerol ink film were used to generated the plot of A*sR*) vs 'dark' time, also illustrated in Figure 11. As before, a quick comparison of the two plots in figure 11, namely absorbance, Abs_{609} (at λ_{max} for Th, i.e. 609 nm; measured spectrophotometrically and taken from the spectral changes in figure 10 and A(*sR*) (calculated as in eqn (1) using *sR* values derived from the digital images in figure 10) vs UV irradiation time reveals that the spectrophotometric absorbance and A(*sR*) data are linearly correlated, as the data points lie on a common line.

As a consequence the two data sets generate the same value for *t(50)*, namely, 4.6 min. Other work shows that *t(50)* is inversely proportion to $\%O_2$ [47].

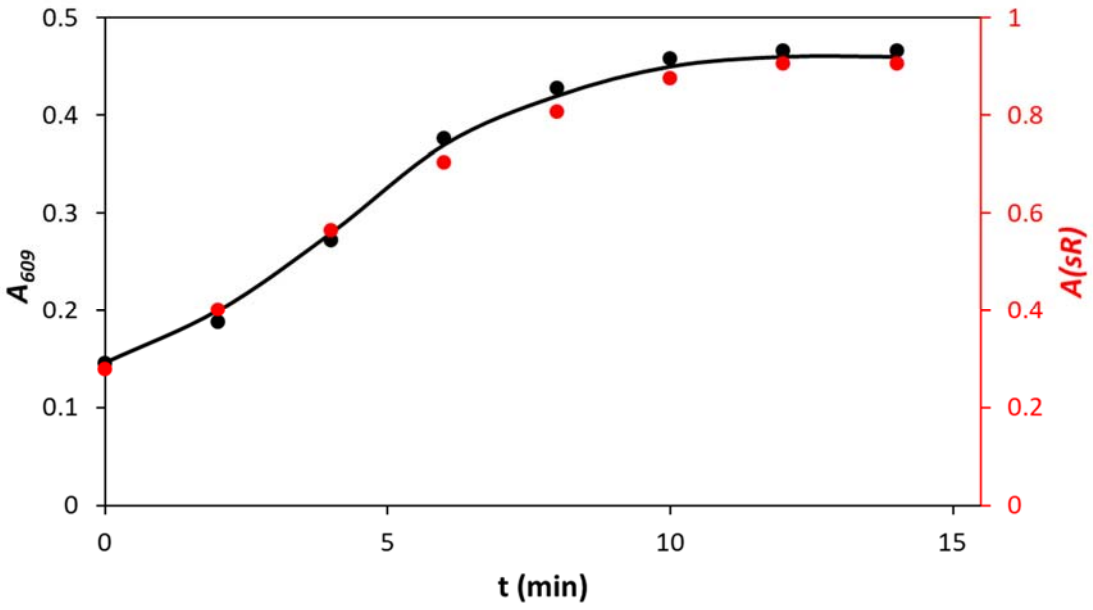

Figure 11: Plots of: (i) absorbance (at λ_{max} Th; measured spectrophotometrically and taken from the spectral changes in figure 9) vs $\%CO_2$ (black data points) and A(*sR*) (calculated as in eqn (1) using *sR* values derived from the digital images in figure 9) vs 'dark' time (red data points). Both data sets identify the same value for *t(50),* namely 4.6 min.

Conclusions

The absorption spectrum of a simple simulated dye, with an absorbance, A_o, at λ_{max} is described by eqn (4). This equation allows the creation of seven absorption spectra, with A_o = 1, that span the visible spectrum. These spectra can be converted into *sRGB* values, see Table 1, which in turn can be used to calculate values for the apparent absorbance, A(*sRGB*), apparent fraction of absorbed light, 1-T(*sRGB*), where T is the apparent transmittance and (iii) colour difference, ΔE. The latter are popular parameters in digital colour colourimetry, DCC. For each dye, one of the *sRGB* colour parameters, the principle colour component, PCC, varies more than the other two as A_o is varied from 0 to 1 (see Table 1) and it is this colour that is used to probe the degree of correlation between actual absorbance (A_o) and the three DCC parameters: A(*sRGB*), 1-T(*sRGB*) and ΔE. For all seven simulated dyes, over the absorbance range 0-1, the apparent absorbance, A(*sRGB*), correlates better with A_o than the other two DCC parameters. Three real indicators, namely: a CO_2 indicator, a photocatalytic activity indicator and an oxygen indicator, were used to test this prediction and in each case the PCC was red. In all three cases the apparent absorbance parameter, A(*sR*), derived from *sRGB* analysis of the digital images, was found to be proportional to the real absorbance, as measured using UV/Vis spectrophotometry, and yielded the same key analytical information, i.e. pCO_2(S=1/2) = 2.7%, *ttb(90)* = 8.6 min and *t(50)* = 4.6 min. In all this work, digital image information capture required only a mobile phone camera and a colour measuring App, and so is much cheaper and easier to use than most UV/Vis spectrophotometers. Although never as good as UV/Vis spectrophotometry, the widespread use of digital cameras and Apps makes it increasingly likely that the use of DCC in quantitative and, especially semi-quantitative, analysis of colour based indicators will become more common place. This work suggests that in most cases the digital data should be plotted in the form of apparent absorbance A(*sRGB*), rather than fractional light absorbed, 1-T(*sRGB*), or colour difference, ΔE. The fact that a digital camera can photograph many indicators simultaneously, suggests that it is also ideally suited for multi-analyte analysis, using an array of colourimetric indicators, unlike UV/Vis spectrophotometry.

References

[1] X.-d. Wang, O.S. Wolfbeis, Fiber-optic chemical sensors and biosensors (2013–2015), Analytical chemistry, 88 (2016) 203-227.

[2] T.R. Knutson, C.M. Knutson, A.R. Mozzetti, A.R. Campos, C.L. Haynes, R.L. Penn, A fresh look at the crystal violet lab with handheld camera colorimetry, Journal of Chemical Education, 92 (2015) 1692-1695.

[3] S. Wang, X. Zhao, I. Khimji, R. Akbas, W. Qiu, D. Edwards, D.W. Cramer, B. Ye, U. Demirci, Integration of cell phone imaging with microchip ELISA to detect ovarian cancer HE4 biomarker in urine at the point-of-care, Lab on a Chip, 11 (2011) 3411-3418.

[4] A. Lapresta-Fernández, L.F. Capitán-Vallvey, Multi-ion detection by one-shot optical sensors using a colour digital photographic camera, Analyst, 136 (2011) 3917-3926.

[5] Y. Zhang, Y. Wu, Y. Zhang, A. Ozcan, Fusion of lens-free microscopy and mobile-phone microscopy images for high-color-accuracy and high-resolution pathology imaging, Optics and Biophotonics in Low-Resource Settings III, International Society for Optics and Photonics, 2017, pp. 100550P.

[6] H. Araki, J. Kim, S. Zhang, A. Banks, K.E. Crawford, X. Sheng, P. Gutruf, Y. Shi, R.M. Pielak, J.A. Rogers, Materials and device designs for an epidermal UV colorimetric dosimeter with near field communication capabilities, Advanced Functional Materials, 27 (2017) 1604465 - 1604474.

[7] G.W. Ewing, Instrumental Methods of Chemical Analysis, 4th ed., McGraw-Hill Inc., Tokyo, Japan, 1975.

[8] Single-beam photometer/filter, http://www.medicalexpo.com/prod/robert-riele/product-69866-675162.html (accessed March 2018).

[9] M.S. Tooms, Colour Reproduction in Electronic Imaging Systems: Photography, Television, Cinematography, John Wiley & Sons, New Delhi, India, 2016.

[10] D.L. Williams, T.J. Flaherty, C.L. Jupe, S.A. Coleman, K.A. Marquez, J.J. Stanton, Beyond λ [lambda] max: transforming visible spectra into 24-bit color values, Journal of Chemical Education, 84 (2007) 1873-1877.

[11] M.A. Stokes, M.; Chandrasekar, S.; Motta, R. , A Standard Default Color Space for the Internet: sRGB Version 1.10, http://www.color.org/sRGB.xalter (Accessed March 2018).

[12] ColorMeter RGB Hex Color Picker and Colorimeter by White Marten, https://itunes.apple.com/us/app/colormeter-rgb-hex-color-picker-and-colorimeter/id713258885?mt=8 (Accessed March 2018).

[13] Color Card and RGB Color Meter by NStart MITech, https://itunes.apple.com/us/app/color-card-and-rgb-color-meter/id1297107041?mt=8 (Accessed March 2018).

[14] Color Mate - Convert and Analyze Colors by David Williames, https://itunes.apple.com/us/app/color-mate-convert-and-analyze-colors/id896088941?mt=8 (Accessed March 2018).

[15] Image J, https://imagej.nih.gov/ij/ (Accessed March 2018).

[16] Adobe Photoshop, https://www.adobe.com/uk/products/photoshop/free-trial-download.html (Accessed March 2018).

[17] Image Colour Picker, https://imagecolorpicker.com/ (Accessed March 2018).

[18] A. Mills, D. Yusufu, Highly CO_2 sensitive extruded fluorescent plastic indicator film based on HPTS, Analyst, 141 (2016) 999-1008.

[19] A. Mills, N. Wells, J. MacKenzie, G. MacDonald, Kinetics of reduction of a resazurin-based photocatalytic activity ink, Catalysis Today, 281 (2017) 14-20.

[20] K Hand Coater, http://rkprint.com/?page_id=10 (Accessed March 2018).

[21] A. Mills, D. Hazafy, Nanocrystalline SnO_2-based, UVB-activated, colourimetric oxygen indicator, Sensors and Actuators B: Chemical, 136 (2009) 344-349.

[22] A. E308-1, Standard Practice for Computing the Colors of Objects by Using the CIE System, ASTM International, West Conshohoken, PA, 2001.

[23] Complementary colours, after-images, retinal fatigue, colour mixing and contrast sensitivity, http://www.animations.physics.unsw.edu.au/jw/light/complementary-colours.htm (Accessed March 2018).

[24] Nellcor™ Adult/Pediatric Colorimetric CO_2 Detector, http://www.medtronic.com/covidien/en-us/products/intubation/nellcor-adult-pediatric-colorimetric-co2-detector.html (Accesses March 2018).

[25] A. Mills, K. Eaton, Optical sensors for carbon dioxide: an overview of sensing strategies past and present, Quimica Analitica, 19 (2000) 75-86.

[26] Presens CO_2-sensors, https://www.presens.de/ (Accessed March 2018).

[27] Ocean Optics, https://oceanoptics.com/(Accessed March 2018).

[28] Mocon, http://www.mocon.com/ (Accessed March 2018).

[29] A. Mills, Q. Chang, N. McMurray, Equilibrium studies on colorimetric plastic film sensors for carbon dioxide, Analytical Chemistry, 64 (1992) 1383-1389.

[30] A. Mills, Q. Chang, Tuning colourimteric and fluorimetric gas sensors for carbon dioxide, Analytica chimica acta, 285 (1994) 113-123.

[31] A. Mills, Optical sensors for carbon dioxide and their applications, in: M.-I. Baraton (Ed.) Sensors for Environment, Health and Security, Springer, UK, 2009, pp. 347-350.

[32] A. Mills, G.A. Skinner, P. Grosshans, Intelligent pigments and plastics for CO 2 detection, Journal of Materials Chemistry, 20 (2010) 5008-5010.

[33] Activ™ glass from Pilkington, https://www.pilkington.com/en-gb/uk/products/product-categories/self-cleaning/pilkington-activ-range (Accessed March 2018).

[34] Climisan paint from STO, http://www.sto.co.uk/en/home/home.html (Accessed March 2018).

[35] TX Active from Italcementi, https://asknature.org/idea/tx-active-cement/#.WquuDX9pxhE (Accessed March 2018).

[36] Hydrotect from TOTO, http://gb.toto.com/technology/technology-single-view/Technology/show/HYDROTECT/(Accessed March 2018).

[37] A. Mills, C. O'Rourke, K. Moore, Powder semiconductor photocatalysis in aqueous solution: An overview of kinetics-based reaction mechanisms, Journal of Photochemistry and Photobiology A: Chemistry, 310 (2015) 66-105.

[38] A. Mills, C. Hill, P.K. Robertson, Overview of the current ISO tests for photocatalytic materials, Journal of Photochemistry and Photobiology A: Chemistry, 237 (2012) 7-23.

[39] A. Mills, J. Wang, S.-K. Lee, M. Simonsen, An intelligence ink for photocatalytic films, Chemical Communications, (2005) 2721-2723.

[40] A. Mills, N. Wells, Reductive photocatalysis and smart inks, Chemical Society Reviews, 44 (2015) 2849-2864.

[41] A. Mills, J. Hepburn, D. Hazafy, C. O'Rourke, N. Wells, J. Krysa, M. Baudys, M. Zlamal, H. Bartkova, C.E. Hill, Photocatalytic activity indicator inks for probing a wide range of surfaces, Journal of Photochemistry and Photobiology A: Chemistry, 290 (2014) 63-71.

[42] A. Mills, N. Wells, Indoor and outdoor monitoring of photocatalytic activity using a mobile phone app. and a photocatalytic activity indicator ink (paii), Journal of Photochemistry and Photobiology A: Chemistry, 298 (2015) 64-67.

[43] ISO/PRF 21066, https://www.iso.org/standard/69815.html (Accessed March 2018).

[44] X.-d. Wang, O.S. Wolfbeis, Optical methods for sensing and imaging oxygen: materials, spectroscopies and applications, Chemical Society Reviews, 43 (2014) 3666-3761.

[45] Oxydot from OxySense, http://www.oxysense.com/(Accessed March 2018).

[46] Spot SP from PreSense, https://www.presens.de/products/o2/sensors.html (Accessed March 2018).

[47] OpTech® O_2 from Mocon, http://www.mocon.com/instruments/optech-o2-model-p.html (Accessed March 2018).

[48] RedEye oxygen sensor patches from OceanOptics, https://oceanoptics.com/product/redeye-oxygen-sensing-patches/ (Accessed March 2018).

[49] S.-K. Lee, A. Mills, A. Lepre, An intelligence ink for oxygen, Chemical communications, (2004) 1912-1913.

[50] S.-K. Lee, M. Sheridan, A. Mills, Novel UV-activated colorimetric oxygen indicator, Chemistry of Materials, 17 (2005) 2744-27.

[51] UPM Shelf Life Guard Keeping an Eye on Packaged Foods, http://www.upm.com/About-us/Newsroom/Releases/Pages/UPM-Shelf-Life-Guard-Keeping-an-Eye-on-Packaged-Foods-001-to-10-helmi-2011-19-14.aspx (Accessed March 2018).